

Common Origin of Warm Dark Matter and Dark Radiation

Manuel A. Buen-Abad,¹ Raymond T. Co,² and Keisuke Harigaya³

¹*Department of Physics, Brown University, Providence, RI, 02912, USA*

²*Leinweber Center for Theoretical Physics,*

University of Michigan, Ann Arbor, MI 48109, USA

³*School of Natural Sciences, Institute for Advanced Study, Princeton, NJ 08540, USA*

(Dated: November 8, 2021)

Abstract

We consider a cosmological scenario where a relativistic particle and a stable massive particle are simultaneously produced from the decay of a late-decaying particle after Big-Bang Nucleosynthesis but before matter-radiation equality. The relativistic and massive particles behave as dark radiation and warm dark matter, respectively. Due to a common origin, the warmness and abundances are closely related. We refer to the models that lead to such a scenario as Common Origin of Warm and Relativistic Decay Products (COWaRD). We show that COWaRD predicts a correlation between the amount of dark radiation and suppression of the large scale structure, which can be tested in future precision cosmology observations. We demonstrate that COWaRD is realized, as an example, in a class of supersymmetric axion models and that future observations by the next generation Cosmic Microwave Background, Large Scale Structure, and 21-cm surveys can reveal the structure of the theory.

CONTENTS

| | |
|--|----|
| 1. Introduction | 3 |
| 2. Cosmological Effects of Dark Radiation and Warm Dark Matter | 5 |
| 2.1. Dark Radiation | 5 |
| 2.2. Warm Dark Matter | 7 |
| 2.3. H_0 and σ_8 tensions | 8 |
| 3. Warm Dark Matter and Dark Radiation as Decay Products | 9 |
| 3.1. Warmness and Abundances | 10 |
| 3.2. Supersymmetric Axion Models | 11 |
| 3.3. Parameter Space with Suppression of σ_8 | 14 |
| 4. Implications for Cosmology | 16 |
| 4.1. Setting and Parameterization | 16 |
| 4.2. The Data | 18 |
| 4.3. Results | 18 |
| A. Production of Axinos and Gravitinos | 21 |
| A.1. Production during Inflationary Reheating | 21 |
| A.2. Production after the Freeze-out of the LOSP | 22 |
| B. MCMC Numerical Results | 23 |
| References | 25 |

1. INTRODUCTION

In the last few decades, cosmology as a science has undergone a phase of accelerated expansion. With the advent of probes of the cosmic microwave background (CMB) as well as experiments mapping the distribution of matter in the Universe [1–7], we are currently living in an era of unprecedented precision in our understanding of the Universe, its composition, and its history.

From all these observations, a “standard” picture has emerged as the best framework to explain the data: the Λ CDM model. In Λ CDM, the majority of the matter in the Universe consists of non-relativistic (“cold”) particles whose dominant interactions among themselves and with the rest of the Universe (the Standard Model of particle physics and the cosmological constant Λ) are through gravity (“dark”). This component has then been appropriately dubbed “cold dark matter” (CDM).

Although the predictions of the Λ CDM model are in outstanding agreement with observational data, cosmological experiments are still far from unambiguously singling out Λ CDM as the only option in town. From the theoretical point of view, the mystery of dark matter (DM) and its properties (origin, mass, spin, interactions, etc.) are perhaps the most common playground for particle physicists interested in cosmology. Many different and well-motivated models have been proposed to explain it, often requiring extra components of the Universe beyond those of vanilla Λ CDM. Furthermore, recent experiments hint to possible cracks in the Λ CDM paradigm. Local measurements of the expansion of the Universe [8–13] and of the large-scale structure (LSS) [2, 5, 6, 14–22] are in disagreement with the predicted values from the fit of Λ CDM to the early Universe data [23–25].

Perhaps the most well-known modifications to the standard Λ CDM model are warm dark matter (WDM) and dark radiation (DR), ubiquitous in well-motivated theoretical frameworks. The sterile neutrino is a popular WDM candidate and can be produced from the thermal scattering processes [26] or the non-thermal resonant conversion [27]. Axions can constitute DR [28] or WDM [29, 30] from parametric resonance, while moduli decays also produce relativistic axions [31–35]. In supersymmetric theories, gravitinos can also constitute WDM and may acquire the relic abundance from scatterings during inflationary reheating [36, 37] or decays of the lightest observable superpartner (LOSP) after freeze-out [38–43]. Similarly, the axinos from reheating [44] or the LOSP decay [45–48] can be WDM. In Twin

Higgs models [49], the twin photons and twin neutrinos also contribute to DR [50–56]. These references consider the presence of either WDM or DR. Remarkably, precision cosmology can reveal information about these new states via gravitational effects alone although their direct interactions may otherwise be too weak for terrestrial experiments.

Certain well-motivated theories predict the simultaneous existence of WDM and DR. In this paper, we point out that precision cosmology can be even more powerful as to reveal the underlying theoretical structure from the correlated signals. We consider a theory where late-decaying particles decay into nearly massless particles and stable massive particles. This predicts that stable particles are WDM that becomes non-relativistic just before the CMB

$$T_{\text{nr}} \simeq 5.5 \text{ eV} \left(\frac{f_{\text{wdm}}}{\Delta N_{\text{eff}}} \right), \quad (1.1)$$

if both the effective number of relativistic species ΔN_{eff} due to the nearly-massless particles and the fractional amount of such warm dark matter f_{wdm} are of the same order. We call such models Common Origin of Warm and Relativistic Decay Products (COWaRD). If the decay products have sufficient interactions with the Standard Model, the required formation of light elements strongly constrains the decay to occur before Big-Bang Nucleosynthesis (BBN). In this case, the thermal interactions tend to equilibrate the decay products and remove the correlation in the signals. On the other hand, if the decay products are invisible, the decay can occur any time before recombination and both WDM and DR survive and leave imprints on the CMB via gravitational effects. These final states can be produced from two different decay channels or in a single decay process; the branching ratio determines the relative abundance for the former case, whereas Eq. (1.1) is applicable to the latter. An example for the former case is the decay of the saxion into a pair of axions or a pair of axinos. For the latter case, examples include the axino/gravitino decay into the gravitino/axino and an axion $\tilde{a}/\tilde{G} \rightarrow \tilde{G}/\tilde{a} a$ as well as the saxion decay into the axino and the gravitino $s \rightarrow \tilde{a}\tilde{G}$. Due to the common origin, their relative abundance is fixed. For concreteness, we will interpret results in the scenario where $\tilde{a}/\tilde{G} \rightarrow \tilde{G}/\tilde{a} a$ is the origin of warm gravitino/axino dark matter and axion dark radiation. Here we comment on previous works on the decaying axino or gravitino. Ref. [57] focuses on DR aspects, while Refs. [58, 59] point out effects on matter spectrum, but no numerical analysis is performed. Contrary to a decay before recombination, Ref. [60] considers lifetimes as long as the age of the universe.

In this work, we investigate the impact this common origin of WDM and DR has on

cosmology. We implement this model into the CLASS Boltzmann solver [61] and perform fits to observational data via Monte-Carlo Markov Chain scans of the available parameter space using MontePython [62, 63]. We find that this model marginally improves the fit to the data compared to Λ CDM, and it establishes an anti-correlation between the amount of DR and the amplitude of the matter fluctuations at large scales, parameterized by σ_8 . As a consequence of this, the detection of extra relativistic degrees of freedom by Stage-4 CMB surveys immediately imply, in the context of the COWaRD model, a value of σ_8 smaller than the prediction from Λ CDM.

The paper is organized as follows. In Sec. 2, we review the qualitative explanations of how WDM and DR affect the CMB and the matter power spectrum. In Sec. 3, we discuss explicit models that give rise to both WDM and DR via perturbative decays and derive the correlation between observables as a result of this common origin. In Sec. 4, we fit the proposed models to the cosmological data sets and provide the interpretation of the results.

2. COSMOLOGICAL EFFECTS OF DARK RADIATION AND WARM DARK MATTER

In this section, we recall how dark radiation and warm dark matter affect cosmological observables. For reviews of this topic, see *e.g.* [64].

2.1. Dark Radiation

Dark radiation is the radiation component of the universe in addition to the prediction of the Standard Model—photons and neutrinos. The abundance of the radiation in addition to photons is commonly parametrized by the effective number of neutrinos N_{eff} ,

$$\rho_{\text{rad}} - \rho_\gamma = N_{\text{eff}} \frac{\pi^2}{30} \frac{7}{4} \left(\frac{4}{11} \right)^{4/3} T_\gamma^4, \quad (2.1)$$

where T_γ is the temperature of photons. The Standard Model prediction is $N_{\text{eff}} \simeq 3.046$ [65, 66] and the DR abundance is parametrized by the deviation from it,

$$\Delta N_{\text{eff}} = N_{\text{eff}} - 3.046. \quad (2.2)$$

The effects of DR on the CMB are well understood [67–70].

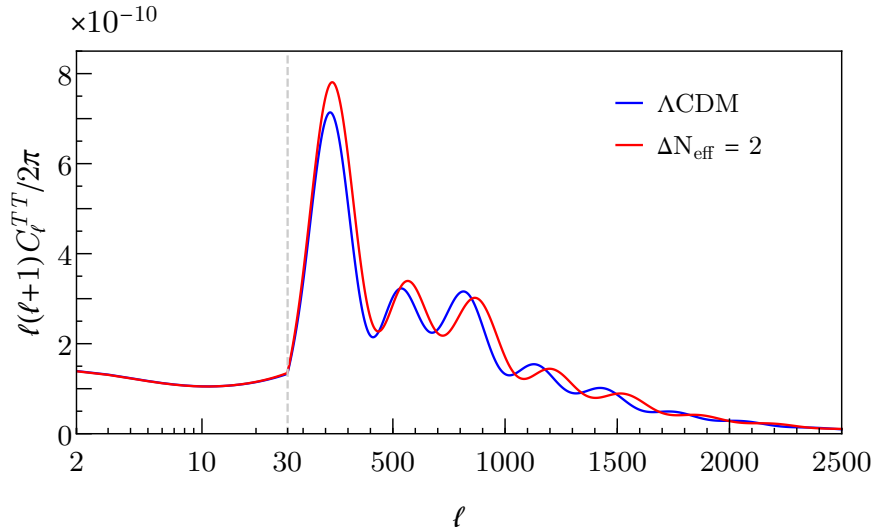


FIG. 1. The effect of dark radiation on the CMB TT spectrum. The blue curve is for Λ CDM with best fit parameters from Planck 2018. In the red curve, two additional relativistic degrees of freedom are introduced to Λ CDM. The scale of the horizontal axis changes from logarithmic to linear at $\ell = 30$.

In Fig. 1, we show the CMB TT spectra for Λ CDM and $+\Delta N_{\text{eff}}$ computed by CLASS [61]. Here we use the best fit cosmological parameters of Λ CDM determined by Planck 2018 $TT+TE+EE+lensing$ and BAO data and fix $h = 0.6766$. The positive ΔN_{eff} affects the CMB spectrum and determination of the cosmological parameters in the following way.

Dark radiation increases the energy density of the universe for a given photon temperature and hence increases the expansion rate of the universe. The sound horizon, $r_s \sim c_s t$, around recombination becomes shorter, where c_s is the sound speed. The angular position of the acoustic peaks of the CMB spectrum moves toward higher multipoles. The angular position of the acoustic peaks is precisely measured by the observations of the CMB. To fix it at the correct position, the distance between us and the last scattering surface is required to be shorter. The distance is basically determined during the cosmological constant dominated era, and inversely proportional to H_0 . Therefore, H_0 estimated from CMB observations becomes larger.

After fixing the positions of the peaks by increasing H_0 , Silk damping [71–75] begins from lower multipoles (a larger expansion rate shortens the diffusion length, but this effect is subdominant). This can be partially compensated by 1) a larger spectral index n_s , which

increases the primordial perturbation at small scales or 2) more baryons which shorten the diffusion length, although too large of a ΔN_{eff} twists the overall shape. Furthermore, the polarization spectra have more power at high multipoles, which helps constrain ΔN_{eff} . Planck 2018 TT+TE+EE+lensing and BAO data set the constraint [23]

$$\Delta N_{\text{eff}} < 0.28 \text{ (95\%C.L.)}. \quad (2.3)$$

Stage-4 ground-based CMB experiments are projected to reach values of $\Delta N_{\text{eff}} \approx 0.03$ [76].

The constraint (2.3) assumes that DR exists before the beginning of Big-Bang Nucleosynthesis (BBN). In this case, since the expansion rate of the universe becomes larger around BBN, the neutron-proton conversion becomes relatively inefficient, making the neutron-to-proton ratio and hence the Helium fraction larger. Helium atoms have large binding energy than protons and recombine with electrons more efficiently. The scattering between CMB photons and electrons becomes less efficient, and the diffusion length of the CMB photons becomes longer. Silk damping begins from yet lower multipoles, strengthening the constraint on ΔN_{eff} . Thus, if DR is produced after BBN, the constraint on ΔN_{eff} is weaker than the one in Eq. (2.3).

If matter-radiation equality is delayed by a positive ΔN_{eff} , the decay of the gravitational potential, which induces the acoustic oscillation, lasts longer. As a result, the amplitude of the first few acoustic peaks becomes larger. (The amplitude of the acoustic peaks at high multipoles is suppressed because of the shift of the peaks to higher multipoles and more effective Silk damping.) This effect should be compensated by larger matter components.

Dark radiation also affects the matter spectrum. In order to keep the time of matter-radiation equality fixed (which is well measured by CMB surveys), an increase in the amount of radiation must be compensated by a corresponding increase in the amount of matter. This in turn translates into a larger matter power spectrum.

2.2. Warm Dark Matter

Warm dark matter is a component of the universe whose energy density is dominated by a mass density around matter-radiation equality but has a large enough velocity dispersion to affect observations. Warm dark matter behaves in the same manner as cold dark matter at the background level, but differently at the perturbation level.

Warm dark matter freely streams and escapes from overdense regions, suppressing the perturbations at length scales shorter than the free-streaming length,

$$\lambda_{\text{FS}} = \int \frac{v(t)}{a(t)} dt \simeq \frac{v(t_{\text{eq}})}{a(t_{\text{eq}})} t_{\text{eq}} \simeq 1 \text{ Mpc} \left(\frac{100 \text{ eV}}{T_{\text{nr}}} \right), \quad (2.4)$$

where T_{nr} is the temperature around which WDM becomes non-relativistic.

The observed shortest scale in the CMB is about 10 Mpc. The observation of the CMB spectrum can constrain the abundance of WDM if $T_{\text{nr}} \lesssim 10 \text{ eV}$.

For larger T_{nr} , the effect of WDM can be observed in the matter power spectrum at small scales, which is measured by galaxy counting, Lyman- α power spectrum, and the Sunyaev-Zel’dovich and lensing effects on the CMB.

2.3. H_0 and σ_8 tensions

While undoubtedly very successful, the Λ CDM model is far from being singled out as the one and only option to explain the available cosmological observations. What is more, there are some indications that Λ CDM is not the whole story. In particular, the values of the Hubble expansion rate H_0 and the amplitude σ_8 of matter fluctuations at the scale of 8 Mpc, as quantities derived from the fit of Λ CDM to the CMB data from the Planck satellite, are in tension with direct measurements of the same.

Indeed, direct measurements of the expansion rate of the Universe tend to yield a large value of H_0 , whereas “indirect” measurements (*i.e.* deductions from Λ CDM fits to data) favor smaller values [8–13, 23–25]. For some of these observations, the tension reaches $4 - 6\sigma$ [77–80]. If this discrepancy is a sign of new physics and not of unaccounted for systematics, the most accepted models that can alleviate this tension are those that change the size of the comoving sound horizon at the time of recombination [77–79]. The most straightforward way to do this is by adding some extra energy density at early times [81–87]¹, such as DR [90–94]. As is explained above, the data is highly sensitive to the behavior of the cosmological perturbations in this extra component, and the simple addition of DR cannot fully explain the tension, as can be seen from the result of Planck 2018 [23].

On the other hand, direct measurements of LSS observe a smaller value of σ_8 than the Λ CDM prediction from its fit to the CMB data [2, 5, 6, 14–23]. The suppression of structure by WDM can explain the discrepancy. For works inspired by the σ_8 problem, see [91–104].

¹ However, see also [88, 89].

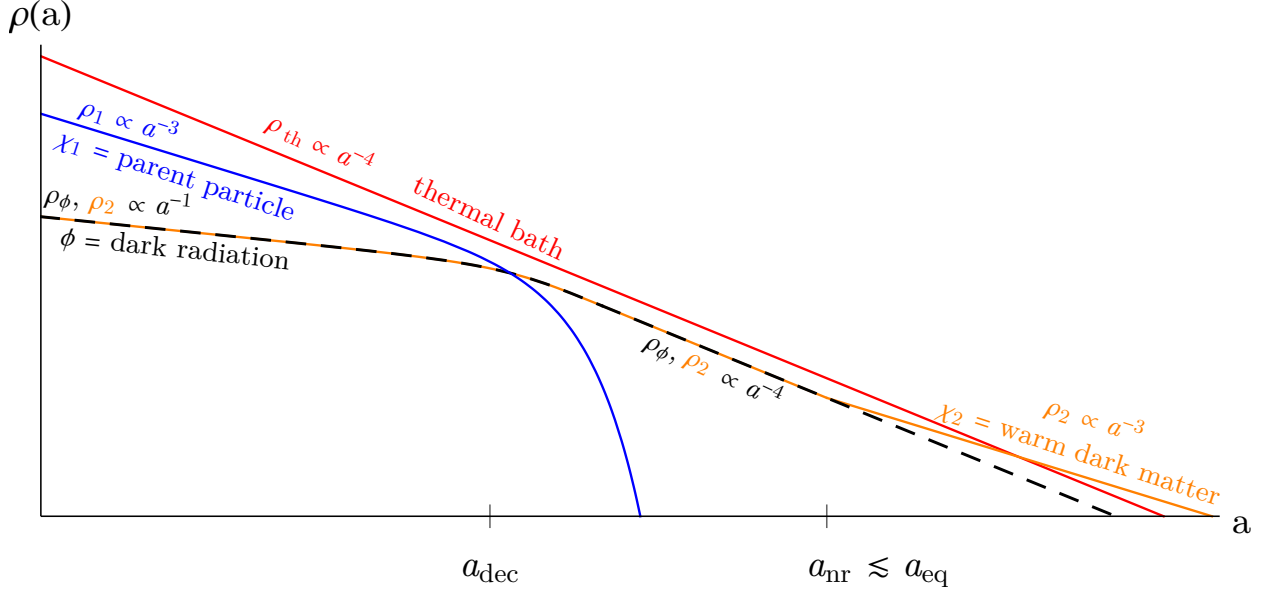


FIG. 2. The evolution of the energy densities ρ with the scale factor a on log-log scales for models of a common origin of WDM and DR. The red line shows the Standard Model thermal bath, while the blue curve is for the parent particle χ_1 decaying into WDM χ_2 (orange) and DR ϕ (black dashed curve). The decay occurs at a_{dec} , while a_{nr} —the scale factor when χ_2 becomes non-relativistic—is close to matter-radiation equality a_{eq} .

3. WARM DARK MATTER AND DARK RADIATION AS DECAY PRODUCTS

Here we consider the scenario where a late-decaying particle χ_1 is produced in the early universe, and later decays into a stable particle χ_2 and a stable and nearly massless particle ϕ . χ_2 may behave as a WDM component or DR depending of the parameter space, and ϕ behaves as DR. In Fig. 2, we demonstrate a cosmological evolution that leads to both WDM and DR. The existence of a sizable fraction of WDM and DR requires that 1) the decay occur when ρ_1 is $\mathcal{O}(0.1)$ fraction of the thermal bath energy density and 2) χ_2 become non-relativistic shortly before matter-radiation equality. As we will show in this section, this scenario is realized in well-motivated models. On the other hand, if the requirement 1) is violated, the abundances of χ_2 and ϕ are negligible or overproduced, while χ_2 is cold dark matter or dark radiation if 2) is violated.

3.1. Warmness and Abundances

The Boltzmann equations of these particles read

$$\dot{\rho}_1 + 3H\rho_1 = -\Gamma\rho_1 \quad (3.1a)$$

$$\dot{\rho}_2 + 4H\rho_2 = \frac{1}{2}\Gamma\rho_1 \quad (3.1b)$$

$$\dot{\rho}_\phi + 4H\rho_\phi = \frac{1}{2}\Gamma\rho_1. \quad (3.1c)$$

For a radiation-dominated universe, the Hubble expansion rate is $H = 1/2t$ and the solutions are given by

$$\rho_1(t) = \rho_1(t_i) \left(\frac{t_i}{t}\right)^{3/2} e^{-\Gamma(t-t_i)} \quad (3.2)$$

$$\rho_{2,\phi}(t) = \rho_1(t_i) \left(\frac{t_i}{t}\right)^{3/2} \frac{\sqrt{\pi}}{4\sqrt{t\Gamma}} \quad \text{for } t_i \ll \Gamma^{-1} \quad \text{and} \quad t \gg \Gamma^{-1}, \quad (3.3)$$

where $\rho_2(t) = \rho_\phi(t)$ until χ_2 becomes non-relativistic. We parametrize the energy density of DR ϕ by the usual effective degrees of freedom ΔN_{eff} so that

$$\rho_\phi = \Delta N_{\text{eff}} \frac{\pi^2 7}{30 4} \left(\frac{4}{11}\right)^{\frac{4}{3}} T^4. \quad (3.4)$$

The energy density of ϕ originates from the decay of χ_1 at temperature T_{dec} and thus

$$\Delta N_{\text{eff}} = \frac{30 4}{\pi^2 7} \left(\frac{11}{4}\right)^{\frac{4}{3}} \frac{\rho_\phi}{T^4} = \left(\frac{11}{4}\right)^{\frac{4}{3}} \frac{4\sqrt{2\pi}g_*(T_{\text{dec}})}{21} \frac{\rho_1/s}{T_{\text{dec}}}, \quad (3.5)$$

where g_* is the effective number of degrees of freedom in the thermal bath, s is the entropy density, and the decay temperature is defined by $H(T_{\text{dec}}) = 1/2t_{\text{dec}} \equiv \Gamma$. We use $\rho_\phi(T_{\text{dec}})/s(T_{\text{dec}}) = \rho_1(T_i)/s(T_i)\sqrt{\pi/8}$ for an initial temperature $T_i \gg T_{\text{dec}}$, which follows from the analytic solutions of the full Boltzmann equations given in Eq. (3.2). We further simplify the notation $\rho_1(T_i)/s(T_i) = \rho_1/s$ because this ratio is a constant for any $T_i \gg T_{\text{dec}}$. Similarly, the number density of χ_2 is equal to that of χ_1 at the time of decay,

$$\left.\frac{\rho_2}{s}\right|_{T=0} = \frac{m_2 n_2}{s} = \frac{\rho_1}{s} \frac{m_2}{m_1}, \quad (3.6)$$

while $m_2 n_2/s$ stays constant afterwards and stands for the energy density of χ_2 at the zero temperature, *i.e.* $\rho_2|_{T=0}$. Lastly, the momentum of χ_2 at $T_{\text{CMB}} \simeq 0.25$ eV can be obtained from that at T_{dec}

$$\left.\frac{p_2}{m_2}\right|_{\text{CMB}} = \frac{p_{\text{dec}}}{m_2} \frac{T_{\text{CMB}}}{T_{\text{dec}}} = \frac{m_1}{2m_2} \frac{T_{\text{CMB}}}{T_{\text{dec}}}, \quad (3.7)$$

where $p_{\text{dec}} = m_1/2$ is a result of the four-momentum conservation assuming $m_2, m_\phi \ll m_1$. Equivalently, χ_2 becomes non-relativistic at the temperature

$$T_{2,\text{nr}} = T_{\text{CMB}} \left. \frac{m_2}{p_2} \right|_{\text{CMB}} = \frac{2m_2}{m_1} T_{\text{dec}}. \quad (3.8)$$

Now with Eqs. (3.5)-(3.7), we can see the dependence of the velocity of χ_2 on the amounts of dark radiation, ΔN_{eff} , and warm dark matter, $\rho_2/s|_{T=0}$,

$$\left. \frac{p_2}{m_2} \right|_{\text{CMB}} = \left(\frac{4}{11} \right)^{\frac{4}{3}} \frac{21}{8\sqrt{2\pi}g_*(T_{\text{dec}})} \frac{\Delta N_{\text{eff}} T_{\text{CMB}}}{\rho_2/s|_{T=0}}. \quad (3.9)$$

Therefore, χ_2 becomes non-relativistic at the temperature

$$T_{2,\text{nr}} = \left(\frac{11}{4} \right)^{\frac{4}{3}} \frac{8\sqrt{2\pi}g_*(T_{\text{dec}})}{21} \frac{\rho_2/s|_{T=0}}{\Delta N_{\text{eff}}} \simeq 5.5 \text{ eV} \left(\frac{f_{\text{wdm}}}{\Delta N_{\text{eff}}} \right), \quad (3.10)$$

which is interestingly just before the CMB epoch when ΔN_{eff} and f_{wdm} are of the similar order. Here, $f_{\text{wdm}} \equiv \rho_2/\rho_{\text{DM}}$ is the abundance of WDM χ_2 in units of the total dark matter abundance today. However, this is merely a result of the fact that the CMB decoupling temperature is close to the temperature of matter-radiation equality. A common origin of WDM and DR necessarily implies that two species have the same number density and the same momentum when relativistic. It is when χ_2 becomes non-relativistic that the two energy densities start to deviate. If this occurs at the CMB epoch, then the two species still have roughly the same energy densities at the CMB and furthermore $\Delta N_{\text{eff}} \simeq \mathcal{O}(1)$ is equivalent to $\rho_2/s|_{T=0} \simeq \rho_{\text{DM}}/s$ due to matter-radiation equality. COWaRD in principle involves three parameters, T_{dec} , f_{wdm} , and ΔN_{eff} . However, if the decay occurs well before the CMB, T_{dec} becomes irrelevant so f_{wdm} and ΔN_{eff} are sufficient to fully describe COWaRD.

3.2. Supersymmetric Axion Models

In this section, we will study supersymmetric axion theories because both supersymmetry and the axion are well motivated to solve outstanding issues in the Standard Model. Supersymmetry provides a solution to the electroweak hierarchy problem [105–108], a framework for precise gauge coupling unification [109–114], and stable massive particles as dark matter candidates [107, 115, 116]. On the other hand, a vanishing neutron electric dipole moment calls for an explanation, known as the strong CP problem [117]. A dynamical solution is

provided by the Peccei-Quinn mechanism [118, 119], where a hypothetical particle called the axion [120, 121] relaxes to a CP-conserving minimum in the potential and cancels the bare strong CP angle in the theory. The axion is a dark matter candidate [122–124], and furthermore may explain the baryon asymmetry of the Universe [125–129]. In supersymmetric axion theories, the Peccei-Quinn symmetry breaking scale can be determined by the dimensional transmutation through the running of the soft mass of the Pecce-Quinn symmetry breaking field [130] or by balance between a negative soft mass term and a higher dimensional term of the Pecce-Quinn symmetry breaking field [131].

In the context of supersymmetric axion theories, we explore explicit models that give rise to both warm dark matter χ_2 and dark radiation ϕ via a perturbative decay $\chi_1 \rightarrow \chi_2 + \phi$. One interesting scenario is the decay of axinos to gravitinos or vice versa, and both decay directions come with axions. The WDM candidate χ_2 is then the gravitino [107] or the axino [45, 46], while the axion produced from the decay behaves as dark radiation ϕ . The decay can safely occur after BBN since the decay products have negligible interactions with the Standard Model. Previous works [58, 59] provide qualitative discussions, while we give a fully quantitative analysis in Sec. 4. In addition, Refs. [58, 59] consider the spectrum where the axino is (much) lighter than the gravitino. The axino and gravitino masses are highly model dependent [132–136] and can also be of the same order in realistic models. For example, the axino can acquire a mass at one loop level via the heavy (s)quarks in KSVZ models, which allows the axino to be heavier than the gravitino in gauge mediation when the PQ breaking scale is below the messenger scale. On the other hand the axino can be massless at the tree level for no-scale supersymmetry, resulting in the axino much lighter than the gravitino. Due to this model uncertainty, we treat the gravitino and axino masses as free parameters.

In what follows, we will show that the decay rate with well-motivated ranges of parameters leads to a relativistic species as well as a warm species that becomes non-relativistic shortly before the CMB epoch. The amounts of produced DR and WDM depend on the abundance of the parent particle at the time of the decay as shown in Eqs. (3.5) and (3.6). The abundance is determined by physics at the high temperatures, such as scatterings during inflationary reheating and freeze-out processes around the TeV scales. We defer the discussion of parent particle’s relic abundance to App. A and simply assume the desired abundance in this section.

We will first focus on the decay of axinos to gravitinos, which is relevant when $m_{\tilde{a}} > m_{3/2}$, and the decay rate is given by

$$\Gamma_{\tilde{a} \rightarrow \tilde{G}a} = \frac{m_{\tilde{a}}^5}{96\pi m_{3/2}^2 M_{\text{Pl}}^2} \left(1 - \frac{m_{3/2}}{m_{\tilde{a}}}\right)^2 \left(1 - \left(\frac{m_{3/2}}{m_{\tilde{a}}}\right)^2\right)^3, \quad (3.11)$$

where the reduced Planck mass $M_{\text{Pl}} = 2.4 \times 10^{18}$ GeV. The decay of axinos dominantly occurs when the decay rate is comparable to the Hubble rate, occurring at a temperature

$$T_{\tilde{a} \rightarrow \tilde{G}a} = \left(\frac{5}{2g_*(T_{\tilde{a} \rightarrow \tilde{G}a})}\right)^{\frac{1}{4}} \frac{m_{\tilde{a}}^{5/2}}{4\pi\sqrt{M_{\text{Pl}}m_{3/2}}} \simeq 4 \text{ eV} \left(\frac{m_{\tilde{a}}}{6 \text{ GeV}}\right)^{\frac{5}{2}} \left(\frac{1 \text{ GeV}}{m_{3/2}}\right) \left(\frac{4}{g_*(T_{\tilde{a} \rightarrow \tilde{G}a})}\right)^{\frac{1}{4}}, \quad (3.12)$$

assuming a radiation-dominated epoch. With the decay temperature from Eq. (3.12), one only needs to specify the abundance of axino at the time of decay, $\rho_{\tilde{a}}(T_{\text{dec}})/s(T_{\text{dec}})$, in order to obtain the amounts of the axion ΔN_{eff} from Eq. (3.5) and of the gravitino $\rho_{3/2}/s|_{T=0}$ from Eq. (3.6). Using Eq. (3.7), we can now estimate when the gravitino becomes non-relativistic,

$$T_{\tilde{G},\text{nr}} = \frac{2m_{3/2}}{m_{\tilde{a}}} T_{\tilde{a} \rightarrow \tilde{G}a} \simeq 1 \text{ eV} \left(\frac{m_{\tilde{a}}}{6 \text{ GeV}}\right)^{\frac{3}{2}} \left(\frac{4}{g_*(T_{\tilde{a} \rightarrow \tilde{G}a})}\right)^{\frac{1}{4}}. \quad (3.13)$$

The result interestingly only depends on the axino mass but not the gravitino mass. This means that the gravitino can be arbitrarily light, while the gravitino is equally warm during the CMB epoch for an axino mass of order 10-100 GeV. A smaller gravitino mass implies that the gravitino is hotter at the time of the axino decay, while the decay itself occurs earlier so that a longer era of redshift exactly compensates a larger initial gravitino momentum.

Now we discuss the alternative mass spectrum where the gravitino is heavier than the axino. In this case, the gravitino decay sources axino WDM and axion DR with a rate

$$\Gamma_{\tilde{G} \rightarrow \tilde{a}a} = \frac{m_{3/2}^3}{192\pi M_{\text{Pl}}^2} \left(1 - \frac{m_{\tilde{a}}}{m_{3/2}}\right)^2 \left(1 - \left(\frac{m_{\tilde{a}}}{m_{3/2}}\right)^2\right)^3. \quad (3.14)$$

In a radiation-dominated epoch, the gravitino decays at the temperature

$$T_{\tilde{G} \rightarrow \tilde{a}a} = \left(\frac{5}{8g_*(T_{\tilde{G} \rightarrow \tilde{a}a})}\right)^{\frac{1}{4}} \frac{m_{3/2}^{3/2}}{4\pi\sqrt{M_{\text{Pl}}}} \simeq 4 \text{ eV} \left(\frac{m_{3/2}}{25 \text{ GeV}}\right)^{\frac{3}{2}} \left(\frac{4}{g_*(T_{\tilde{G} \rightarrow \tilde{a}a})}\right)^{\frac{1}{4}}, \quad (3.15)$$

and the axino becomes non-relativistic at

$$T_{\tilde{a},\text{nr}} = \frac{2m_{\tilde{a}}}{m_{3/2}} T_{\tilde{G} \rightarrow \tilde{a}a} \simeq 1 \text{ eV} \left(\frac{m_{\tilde{a}}}{4 \text{ GeV}}\right) \left(\frac{m_{3/2}}{25 \text{ GeV}}\right)^{\frac{1}{2}} \left(\frac{4}{g_*(T_{\tilde{G} \rightarrow \tilde{a}a})}\right)^{\frac{1}{4}}. \quad (3.16)$$

In this mass spectrum, the decay occurs before the CMB as long as $m_{3/2} > \mathcal{O}(10)$ GeV, while the axino mass needs to be $m_{\tilde{a}} \simeq \mathcal{O}(10)$ GeV $(30 \text{ GeV}/m_{3/2})^{1/2}$ to obtain WDM.

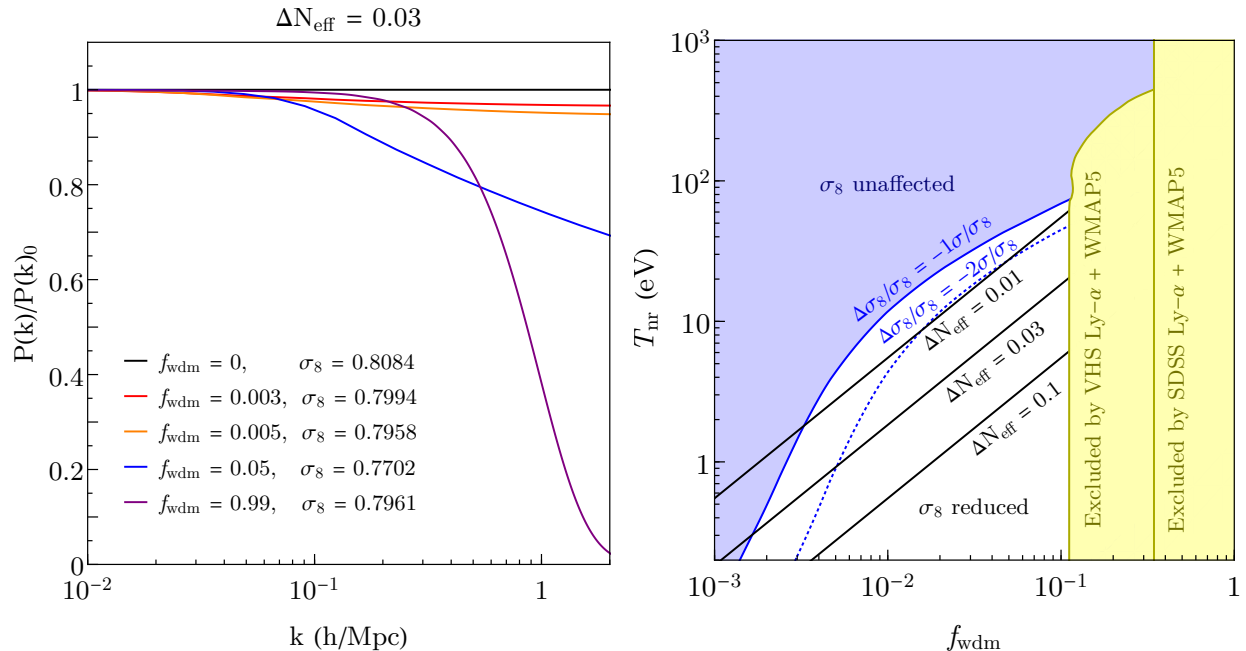


FIG. 3. The suppression of the matter spectrum due to both WDM and DR as decay products. **Left panel:** the relative change compared to cold dark matter in the matter power spectra for various fractional amounts of WDM f_{wdm} . **Right panel:** below the solid (dotted) blue contours σ_8 is significantly suppressed, *i.e.* more than $1(2)\sigma/\sigma_8$ compared to ΛCDM extended by the same amount of ΔN_{eff} as in the COWaRD model (black contours). The yellow region is excluded by Lyman- α constraints [137–140].

3.3. Parameter Space with Suppression of σ_8

The existence of WDM and DR leads to a suppressed matter power spectrum. The effect of WDM on cosmological observables depends on both its abundance and velocity around the CMB epoch. For a given ΔN_{eff} , according to Eq. (3.10), the abundance and warmness of χ_2 are inversely correlated. In the left panel of Fig. 3, we fix $\Delta N_{\text{eff}} = 0.03$ and compute the matter power spectrum as a function of the wavenumber for various values of f_{wdm} . We normalize the spectrum by that of $f_{\text{wdm}} = 0$. For a fixed ΔN_{eff} , a larger f_{wdm} implies colder WDM, whose correlation is given by Eq. (3.10). As f_{wdm} is increased, the matter spectrum is suppressed more. Since the free-streaming length becomes shorter, the suppression occurs only for smaller scales. For $f_{\text{wdm}} \sim 1$, the impact on σ_8 is hence minor, but the power at $k \gtrsim 1 \text{ h/Mpc}$ is significantly suppressed.

We scan over the COWaRD parameters f_{wdm} and T_{nr} and examine the impact on σ_8 . To be rigorous, one should also scan over other cosmological parameters to find the preferred range of parameters for a given $(f_{\text{wdm}}, T_{\text{nr}})$, and predict σ_8 . However, since WDM dominantly affects the prediction of σ_8 without affecting the CMB spectrum much, we can approximately infer the impact in the following way. We compute the ratio of σ_8 obtained in COWaRD containing both WDM and DR to that of ΛCDM extended with the same value of ΔN_{eff} that COWaRD predicts, for fixed ΛCDM cosmological parameters. Using this methodology in the right panel of Fig. 3, we identify the region of parameter space below the solid (dotted) blue contours that leads to a fractional change $(\sigma_8^{\text{COWaRD}} - \sigma_8)/\sigma_8$ more than $1(2)\sigma/\sigma_8 \simeq 0.75(1.5)\%$ where σ and σ_8 are the uncertainty and the measurement of σ_8 by Planck 2018. The yellow region is excluded by Lyman- α constraints [140], which are based on the analyses presented by VHS [137] and for the SDSS experiment [138, 139].

In Fig. 4, for a fixed $\Delta N_{\text{eff}} = 0.03$, we show the parameter space in particle physics models where σ_8 is significantly suppressed with the criterion defined in the methodology we used in Fig. 3. In the left panel, m_1/m_2 is the ratio of the parent and daughter particle masses and T_{dec} is the temperature at which the decay occurs. Warm dark matter and dark radiation lead to a significant (2σ) reduction in σ_8 in the region below the orange line, where 2σ is defined above. The region above the orange line on the other hand has σ_8 unaffected because the WDM abundance is too small despite WDM being very hot. The yellow region is excluded by the observations Lyman- α forests as also shown in Fig. 3. In the red region, the decay occurs after the smallest observed scale in the CMB enters the horizon, and the CMB power spectrum is expected to be distorted in a way different from what a simple addition of WDM and DR does. Although the region may be viable, it is beyond the scope of our present analysis. The blue region leads to too much cold dark matter as inferred by Eqs. (3.7) and (3.9) for a fixed ΔN_{eff} . The right panel is similar except that the parameter space is for the concrete supersymmetric axino/gravitino models elaborated in Sec. 3.2. The black dashed line divides the region into one with a gravitino heavier than the axino (above) and the other with the opposite mass hierarchy. Interestingly, axinos lighter than $\mathcal{O}(30)$ GeV and gravitinos with any mass can lead to the prediction of COWaRD—a nonzero ΔN_{eff} and a suppressed σ_8 .

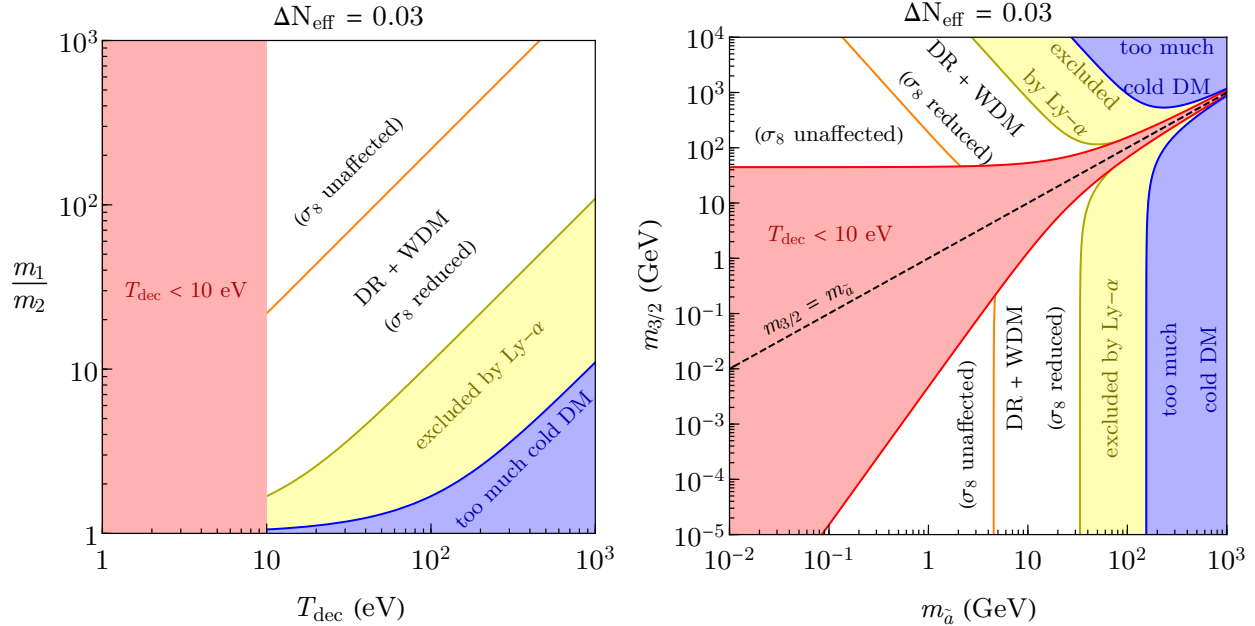


FIG. 4. The region between the orange and yellow curves leads to a significant suppression of the matter power spectrum at 8 Mpc scale σ_8 , in the parameter space of **left panel**: the mass ratio m_1/m_2 between the parent and daughter particles and the decay temperature T_{dec} , **right panel**: the gravitino mass $m_{3/2}$ and the axino mass $m_{\tilde{a}}$.

4. IMPLICATIONS FOR COSMOLOGY

As stated previously, there is currently a plethora of cosmological observations that constrain any extensions to the Standard Model of cosmology ΛCDM . In the model of COWaRD, the main two ingredients beyond those of vanilla ΛCDM are the WDM and DR components, which have a common origin and are related by Eq. (3.9). In this section, we describe the implementation of COWaRD into a code for the evolution of its cosmological perturbations, as well as its fit to the available cosmological data, and explain the results.

4.1. Setting and Parameterization

We first note that there is a wide array of values for the time of decay t_{dec} , deep inside the radiation-dominated era, to which the available cosmological probes measuring the CMB and LSS are not sensitive. In terms of the corresponding scale factor a_{dec} , this range is given by $a_{\text{BBN}} \ll a_{\text{dec}} \ll a_{\text{probed}}$, where $a_{\text{BBN}} \sim 10^{-8}$ is the scale factor at the time of BBN, and

$a_{\text{probed}} \sim 10^{-5}$ corresponds to the earliest time at which the smallest scales measured by the cosmological probes enter the horizon. Indeed for a_{dec} satisfying these inequalities there are (i) no effects of ΔN_{eff} on BBN to speak of, and (ii) no consequences, coming from the decay process itself, on the cosmological observables. We corroborated that indeed the fits to cosmological data are insensitive to a_{dec} within this range and therefore, without loss of generality, we fix $a_{\text{dec}} = 10^{-7}$. A more general implementation of this model, where the decay into WDM and DR is exactly modeled, at both the background and perturbations level and for any value of a_{dec} whatsoever, is beyond the scope of this paper and left to future work.

We implemented the COWaRD model into the Boltzmann code CLASS [61], which already allows for the inclusion of non-cold (*i.e.* warm) dark matter components. To include the WDM we need its phase space distribution function $f(q)$, where $q = ap$ is the comoving momentum of the particles. From the Boltzmann equation with a decay term, we find $f(q)$ to be given by

$$f(q) = \frac{\rho_{2,0}}{m_2} \frac{2\pi^2}{qq_{\text{dec}}^2} e^{-\frac{q^2}{2q_{\text{dec}}^2}} \Theta(p_{\text{dec}} - q) , \quad (4.1)$$

where we define $q_{\text{dec}} \equiv a_{\text{dec}}p_{\text{dec}}$ and $\rho_{2,0} \equiv \rho_2|_{T=0}$ is today's value of the energy density in the massive daughter particles.

As stated above, we fix $a_{\text{dec}} = 10^{-7}$. This simplified version of the COWaRD model is then described by two parameters—the amounts of WDM and of DR. We denote these quantities respectively by $f_{\text{wdm}} \equiv \frac{\rho_{2,0}}{\rho_{\text{DM},0}} = \frac{\rho_{2,0}}{\rho_{2,0} + \rho_{\text{cdm},0}}$, the fraction of DM today that contributed as WDM; and by ΔN_{eff} , given by Eq. (2.2). The warmth of WDM, which is related to the time at which the WDM becomes non-relativistic, can be obtained from these two parameters with Eq. (3.9).

To study the fit of the COWaRD model to current cosmological data we perform parameter scans over ΔN_{eff} and f_{wdm} , in addition to the six standard Λ CDM parameters. We make these scans using the Monte Carlo Markov Chain (MCMC) code `MontePython` version 3.2 [62, 63] with the Metropolis-Hastings algorithm. Our priors on ΔN_{eff} and f_{wdm} are linear and only require these parameters to be non-negative. Finally, we include one massive neutrino of mass $m_\nu = 0.06$ eV.

4.2. The Data

For our MCMC analysis, we use the following data sets:

- **CMB:** We use the published Planck 2018 TT+TE+EE and lensing data [7].
- **BAO:** We include measurements of D_V/r_{drag} by 6dFGS at $z = 0.106$ [1], by SDSS from the MGS galaxy sample at $z = 0.15$ [3], and by BOSS from the CMASS and LOWZ galaxy samples of SDSS-III DR12 at $z = 0.2 - 0.75$ [4].
- **Pantheon:** We also fit to the Pantheon set of type Ia supernovae (SN Ia) [141], which consists of 1048 luminosity distances in the redshift range $0.01 < z < 2.3$. We include the nuisance parameter M for the absolute magnitude of the SN Ia.

Combining the Planck satellite’s measurements of the CMB with BAO and Pantheon has the advantage of narrowing down the values of different parameters, including the sound horizon and the evolution of the energy density of the Universe at late times. There are of course other data sets, perhaps the most prominent being the local measurements of the expansion of the Universe and of the large scale structure [2, 5, 6, 8–25]. However, as we discussed in Sec. 2.3, some of these measurements seem to be in tension with measurements from the Planck satellite, and thus we do not include them in our MCMC analysis.

4.3. Results

We do our numerical analysis for both the standard Λ CDM model and the COWaRD model, fitting their parameters to the cosmological data described in the previous section. We find that the COWaRD model only very marginally improves the fit to the data, with a $\Delta\chi_{\text{eff}}^2 \sim \text{few}$ (see Table I in Appendix B). However, this fit sheds light on some important cosmological predictions of the COWaRD model.

Perhaps the most important consequence of the COWaRD model is the suppression of LSS. Fig. 5 shows the posteriors and likelihoods contours of the σ_8 , Ω_m and f_{wDM} parameters resulting from the MCMC fits to the data. We consider the Λ CDM model, the simplified COWaRD model (parameterized by f_{wDM} and ΔN_{eff} and with $a_{\text{dec}} = 10^{-7}$), and the simplified COWaRD with fixed $\Delta N_{\text{eff}} = 0.03$. Also included for reference in the figure are the 68% and 95% C.L. contours from the Planck SZ cluster counts, which measure $\sigma_8 (\Omega_m/0.27)^{0.3} =$

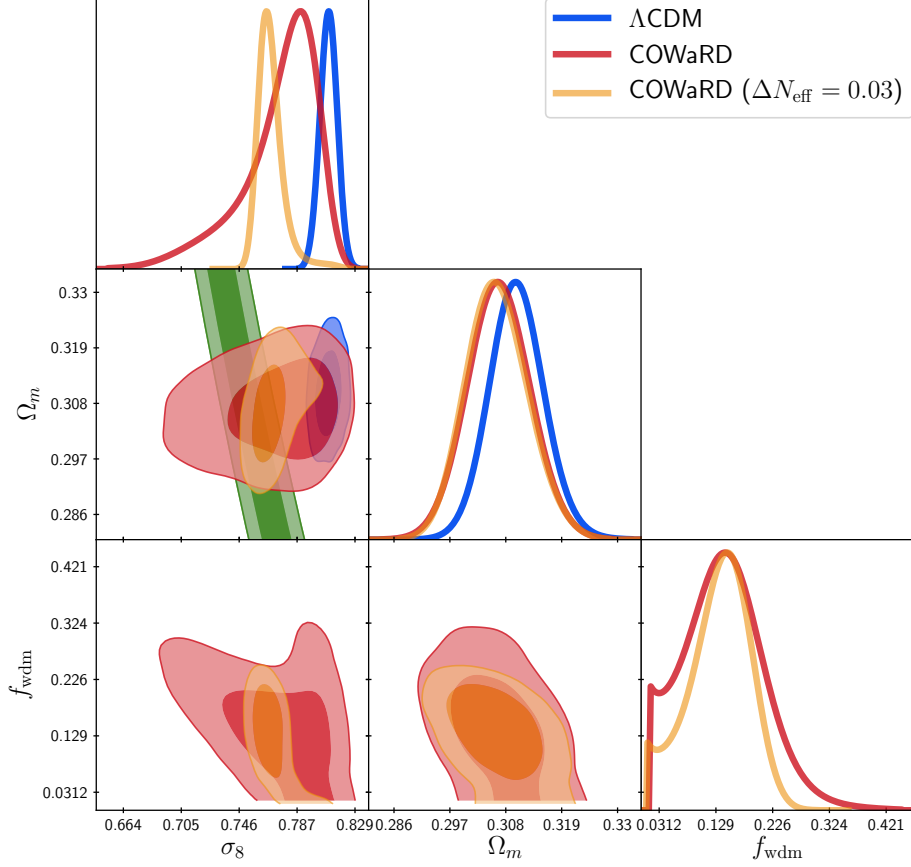


FIG. 5. Posteriors and likelihood contours of the σ_8 , Ω_m and f_{wdm} parameters, from the fit of the ΛCDM (blue), COWaRD (red), and COWaRD with fixed $\Delta N_{\text{eff}} = 0.03$ (yellow) models to the cosmological data. In green are the 68% and 95% C.L. contours from the Planck SZ cluster counts, which measure σ_8 [17].

0.782 ± 0.010 [17]. As mentioned in Sec. 2.3, there is a mild tension between ΛCDM fits to Planck’s CMB data and direct measurements of LSS, which is parameterized by σ_8 [2, 5, 6, 14–23], with Planck predicting a larger σ_8 than warranted by direct observations. As can be seen from the plot, the fit of the COWaRD model to the data automatically allows for smaller values of σ_8 *without having to include the measurements of LSS in the fit*, and, as shown in Table I in Appendix B, without degrading the fit to the cosmological data when compared to ΛCDM .

This brings us to the second consequence of the COWaRD model: ΔN_{eff} and σ_8 are inversely correlated, as can be seen in Fig. 6. This is in sharp contrast to what happens in the “pure DR” $\Lambda\text{CDM} + \Delta N_{\text{eff}}$ extension, where σ_8 and ΔN_{eff} are *positively* correlated [23].

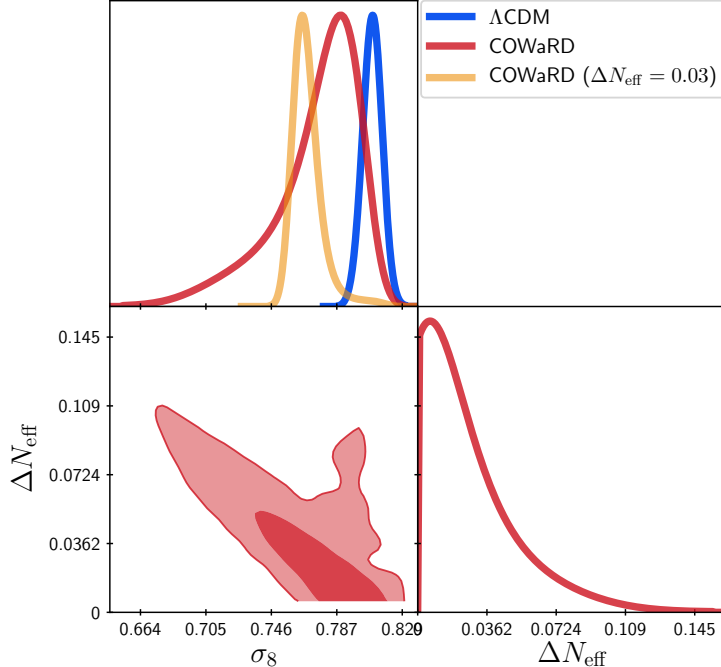


FIG. 6. Posteriors and likelihood contours of the σ_8 and ΔN_{eff} parameters, from the fit of the ΛCDM (blue), COWaRD (red), and COWaRD with $\Delta N_{\text{eff}} = 0.03$ (yellow) models to the cosmological data.

Note that this pure DR limit, when compared to ΛCDM there is only extra DR and no WDM, is not preferred by our fit to the data. This presents us with an exciting prospect: a positive detection of a non-vanishing ΔN_{eff} immediately implies, within the COWaRD model, a value of σ_8 smaller than the one predicted by ΛCDM ; and vice versa. Future S4-CMB experiments will reach the threshold $\Delta N_{\text{eff}} \approx 0.03$ [76], whereas next-generation LSS such as LSST and EUCLID [142, 143] surveys will measure σ_8 and Ω_m more precisely and decide the issue of the LSS tension. For example, were a value of $\Delta N_{\text{eff}} = 0.03$ to be discovered, the fit to the data of the COWaRD model boldly predicts $\sigma_8 = 0.769^{+0.006}_{-0.01}$ (see Table II in Appendix B).

COWaRD can be further probed by measurements of the matter power spectrum at smaller scales. The 1σ preferred values of f_{wDM} is above 0.05 for $\Delta N_{\text{eff}} = 0.03$. As can be seen in the left panel of Fig. 3, the matter power spectrum at $k \gg 1 \text{ h/Mpc}$ is suppressed more than 40%. This large suppression can be detected by future measurements of 21-cm power spectrum [144–148].

Acknowledgments.—We thank Lawrence Hall, Benjamin Horowitz, and Kathryn Zurek for collaboration in the early stages of this work and David Pinner for useful discussions. Part of this research was conducted using computational resources and services at the Center for Computation and Visualization at Brown University. M.B.A. would like to thank Boston University for its hospitality, and the Boston University Shared Computing Cluster (SCC) in the MGHPCC for the computing resources used in the early stages of this project. The work was supported in part by the NASA grant 80NSSC18K1010 (M.B.A.), the DoE Early Career Grant DE-SC0019225 (R.C.), the DoE grant DE-SC0009988 (K.H.) and the Raymond and Beverly Sackler Foundation Fund (K.H.).

Appendix A: Production of Axinos and Gravitinos

In this appendix, we review the computation of the relic abundance of the axino and the gravitino before decaying into WDM and DR. We assume that reheating after inflation completes at a temperature T_{RH} , and the universe is radiation dominated until the standard matter-radiation equality.

A.1. Production during Inflationary Reheating

Axinos couple to gluons and gluinos by a dimension-5 coupling suppressed by the scale $\sim 4\pi f_a/\alpha$ with f_a the axion decay constant. Axinos are then dominantly produced around $T = T_{\text{RH}}$. The number density of axinos normalized by the entropy density s is [44]

$$\left(\frac{n_{\tilde{a}}}{s}\right)_{\text{RH}} \simeq 2 \times 10^{-11} \left(\frac{T_{\text{RH}}}{10^4 \text{ GeV}}\right) \left(\frac{10^{13} \text{ GeV}}{f_a}\right)^2, \quad (\text{A.1})$$

which implies that the required reheat temperature is

$$T_{\text{RH}} \simeq 20 \text{ TeV} \left(\frac{f_{3/2}}{0.1}\right) \left(\frac{\text{GeV}}{m_{3/2}}\right) \left(\frac{f_a}{10^{13} \text{ GeV}}\right)^2, \quad (\text{A.2})$$

in order to generate the amount of gravitino WDM in units of total dark matter abundance, $f_{3/2} \equiv \Omega_{3/2}/\Omega_{\text{DM}}$.

Gravitinos couple to gluons and gluinos by a dimension-5 coupling suppressed by a scale $\sim m_{3/2}M_{\text{Pl}}/m_{\tilde{g}}$ with $m_{\tilde{g}}$ the gluino mass. Gravitinos are also dominantly produced around

$T = T_{\text{RH}}$, resulting in the number density [36, 37]

$$\left(\frac{n_{3/2}}{s}\right)_{\text{RH}} \simeq 4 \times 10^{-9} \left(\frac{25 \text{ GeV}}{m_{3/2}}\right)^2 \left(\frac{T_{\text{RH}}}{10^{11} \text{ GeV}}\right) \left(\frac{m_{\tilde{g}}}{\text{TeV}}\right)^2. \quad (\text{A.3})$$

To produce $f_{\tilde{a}} \equiv \Omega_{\tilde{a}}/\Omega_{\text{DM}}$ fraction of dark matter in warm axinos, the required reheat temperature is

$$T_{\text{RH}} \simeq 3 \times 10^8 \text{ GeV} \left(\frac{f_{\tilde{a}}}{0.1}\right) \left(\frac{4 \text{ GeV}}{m_{\tilde{a}}}\right) \left(\frac{m_{3/2}}{25 \text{ GeV}}\right)^2 \left(\frac{\text{TeV}}{m_{\tilde{g}}}\right)^2. \quad (\text{A.4})$$

If correlated signals in ΔN_{eff} and σ_8 are detected, one can therefore infer the values of the reheat temperature after inflation by Eqs. (A.2) and (A.4). The discussion in this section assumes radiation domination between the end of reheating until matter-radiation equality. The required reheat temperature can be much higher if there exists a matter-dominated epoch, which dilutes the relic abundance with entropy production. For example, Refs. [149–155] consider the case where a matter-dominated era originates from the condensate of the Pecci-Quinn symmetry breaking field.

A.2. Production after the Freeze-out of the LOSP

The lightest particle among the superpartners of the Standard Model particles other than the graviton is called the lightest observable supersymmetric particle (LOSP). After the LOSP abundance is fixed by the freeze-out process, it decays into the gravitino or the axino. This contribution can dominate over the above contribution if the LOSP annihilation is ineffective, which is the case for the bino-like LOSP. Assuming that the annihilation rate is dominated by t-channel exchange of nearly-degenerated right-handed sleptons $\tilde{\ell}_R$, the number density of the bino after the freeze-out is given by [156]

$$\frac{n_{\tilde{B}}}{s} \simeq 2 \times 10^{-10} \left(\frac{m_{\tilde{\ell}_R}}{4 \text{ TeV}}\right)^4 \left(\frac{2 \text{ TeV}}{m_{\tilde{B}}}\right)^3. \quad (\text{A.5})$$

After the chain of decays $\tilde{B} \rightarrow \tilde{a}/\tilde{G} \rightarrow \tilde{G}/\tilde{a}$, this results in a fractional abundance of WDM in units of total dark matter abundance,

$$\frac{\Omega_{\text{wdm}} h^2}{\Omega_{\text{DM}} h^2} = 0.5 \left(\frac{m_{\text{wdm}}}{\text{GeV}}\right) \left(\frac{m_{\tilde{\ell}_R}}{4 \text{ TeV}}\right)^4 \left(\frac{2 \text{ TeV}}{m_{\tilde{B}}}\right)^3, \quad (\text{A.6})$$

with m_{wdm} the mass of warm dark matter, the lighter of \tilde{a} and \tilde{G} .

The bino decay rate into the axino is [47]

$$\Gamma_{\tilde{B} \rightarrow \tilde{a} + B} = \frac{\alpha_{\text{EM}}^2 C^2}{128\pi^3 \cos^4 \theta_W} \frac{m_{\tilde{B}}^3}{f_a^2} \left(1 - \frac{m_{\tilde{a}}^2}{m_{\tilde{B}}^2}\right)^3, \quad (\text{A.7})$$

where the model-dependent parameter C depends on the axion coupling with the hyper gauge bosons, the mass mixing of binos, and the Weinberg angle. The temperature at which the decay occurs in a radiation-dominated epoch is given by

$$T_{\tilde{B} \rightarrow \tilde{a} + B} \simeq 10 \text{ MeV } C \left(\frac{m_{\tilde{B}}}{\text{TeV}}\right)^{\frac{3}{2}} \left(\frac{10^{12} \text{ GeV}}{f_a}\right). \quad (\text{A.8})$$

This implies that the gravitino becomes non-relativistic at the temperature

$$T_{\tilde{a}, \text{nr}} \simeq 50 \text{ keV } C \left(\frac{m_{\tilde{B}}}{\text{TeV}}\right)^{\frac{1}{2}} \left(\frac{m_{\tilde{a}}}{6 \text{ GeV}}\right) \left(\frac{10^{12} \text{ GeV}}{f_a}\right). \quad (\text{A.9})$$

As assumed in deriving Eq. (3.13), the axino is non-relativistic when decaying to the gravitino, $T_{\tilde{a}, \text{nr}} > T_{\tilde{a} \rightarrow \tilde{G} a}$, as long as

$$f_a < 10^{16} \text{ GeV } C \left(\frac{m_{\tilde{B}}}{\text{TeV}}\right)^{\frac{1}{2}} \left(\frac{m_{3/2}}{\text{GeV}}\right) \left(\frac{6 \text{ GeV}}{m_{\tilde{a}}}\right)^{\frac{3}{2}}. \quad (\text{A.10})$$

Similarly, the decay rate and the temperature for the bino decay into the gravitino are [47]

$$\Gamma_{\tilde{B} \rightarrow \tilde{G} + Z/\gamma} = \frac{m_{\tilde{B}}^5}{96\pi m_{3/2}^2 M_{\text{Pl}}^2}, \quad (\text{A.11})$$

$$T_{\tilde{B} \rightarrow \tilde{G} + Z/\gamma} \simeq 1 \text{ MeV } \left(\frac{m_{\tilde{B}}}{\text{TeV}}\right)^{5/2} \left(\frac{\text{GeV}}{m_{3/2}}\right). \quad (\text{A.12})$$

and the axino becomes non-relativistic at the temperature

$$T_{3/2, \text{nr}} \simeq \text{keV} \left(\frac{m_{\tilde{B}}}{\text{TeV}}\right)^{\frac{3}{2}}, \quad (\text{A.13})$$

which implies that, in deriving Eq. (3.16), the assumption of a non-relativistic gravitino at the time of the decay, $T_{3/2, \text{nr}} > T_{\tilde{G} \rightarrow \tilde{a} a}$, is valid as long as $m_{\tilde{B}} > m_{3/2}$, which is anyway required by kinematics.

Appendix B: MCMC Numerical Results

In this appendix we summarize the numerical results from the MCMC fits of the Λ CDM and COWaRD models to the cosmological data. Table I presents the χ^2 of the models, and Table II shows the values of the different parameters.

| Best-fit χ^2 | | | |
|-----------------------------|---------------|---------|---|
| Data Sets | Λ CDM | COWaRD | COWaRD ($\Delta N_{\text{eff}} = 0.03$) |
| high- ℓ TTTEEE | 2349.37 | 2346.77 | 2348.88 |
| low- ℓ EE | 395.69 | 396.02 | 395.80 |
| low- ℓ TT | 22.67 | 23.27 | 22.26 |
| lensing | 9.44 | 10.09 | 9.80 |
| Pantheon | 1027.38 | 1027.06 | 1027.16 |
| BAO | 5.50 | 5.17 | 5.30 |
| TOTAL | 3810.04 | 3808.38 | 3809.21 |
| $\Delta\chi_{\text{eff}}^2$ | — | -1.66 | -0.83 |

TABLE I. Minimum *effective chi square* $\chi_{\text{eff}}^2 = -2 \ln \mathcal{L}$ of the Λ CDM and COWaRD models.

| Parameter values | | | |
|-------------------------|--------------------------------|-------------------------------|---|
| Parameter | Λ CDM | COWaRD | COWaRD ($\Delta N_{\text{eff}} = 0.03$) |
| 100 ω_b | $2.244^{+0.014}_{-0.014}$ | $2.253^{+0.015}_{-0.014}$ | $2.253^{+0.014}_{-0.014}$ |
| n_s | $0.9667^{+0.0038}_{-0.0038}$ | $0.9686^{+0.004}_{-0.0041}$ | $0.9685^{+0.004}_{-0.004}$ |
| τ_{reio} | $0.05637^{+0.0071}_{-0.0076}$ | $0.05168^{+0.0081}_{-0.0077}$ | $0.05173^{+0.0079}_{-0.008}$ |
| 100 θ_s | $1.042^{+0.00029}_{-0.00031}$ | $1.042^{+0.00031}_{-0.0003}$ | $1.042^{+0.0003}_{-0.00029}$ |
| $\ln 10^{10} A_s$ | $3.047^{+0.015}_{-0.015}$ | $3.036^{+0.017}_{-0.016}$ | $3.036^{+0.016}_{-0.017}$ |
| ω_{cdm} | $0.1192^{+0.00088}_{-0.00097}$ | $0.103^{+0.0087}_{-0.0095}$ | $0.1036^{+0.0056}_{-0.0085}$ |
| ΔN_{eff} | — | $0.0287^{+0.0061}_{-0.029}$ | 0.03 |
| f_{wdm} | — | $0.1366^{+0.074}_{-0.073}$ | $0.1311^{+0.066}_{-0.044}$ |
| H_0 | $67.76^{+0.42}_{-0.41}$ | $68.19^{+0.47}_{-0.52}$ | $68.2^{+0.46}_{-0.45}$ |
| σ_8 | $0.8097^{+0.0061}_{-0.0062}$ | $0.7745^{+0.036}_{-0.015}$ | $0.7689^{+0.0054}_{-0.0097}$ |
| Ω_m | $0.3099^{+0.0052}_{-0.0059}$ | $0.3064^{+0.0061}_{-0.0064}$ | $0.3062^{+0.0058}_{-0.0064}$ |

TABLE II. Mean values and 68% C.L. intervals of the parameters of the Λ CDM and COWaRD models.

-
- [1] F. Beutler, C. Blake, M. Colless, D. H. Jones, L. Staveley-Smith, L. Campbell, Q. Parker, W. Saunders, and F. Watson, *Mon. Not. Roy. Astron. Soc.* **416**, 3017 (2011), [arXiv:1106.3366 \[astro-ph.CO\]](#).
- [2] C. Heymans *et al.*, *Mon. Not. Roy. Astron. Soc.* **432**, 2433 (2013), [arXiv:1303.1808 \[astro-ph.CO\]](#).
- [3] A. J. Ross, L. Samushia, C. Howlett, W. J. Percival, A. Burden, and M. Manera, *Mon. Not. Roy. Astron. Soc.* **449**, 835 (2015), [arXiv:1409.3242 \[astro-ph.CO\]](#).
- [4] S. Alam *et al.* (BOSS), *Mon. Not. Roy. Astron. Soc.* **470**, 2617 (2017), [arXiv:1607.03155 \[astro-ph.CO\]](#).
- [5] F. Khlinger *et al.*, *Mon. Not. Roy. Astron. Soc.* **471**, 4412 (2017), [arXiv:1706.02892 \[astro-ph.CO\]](#).
- [6] S. Joudaki *et al.*, *Mon. Not. Roy. Astron. Soc.* **474**, 4894 (2018), [arXiv:1707.06627 \[astro-ph.CO\]](#).
- [7] Y. Akrami *et al.* (Planck), (2018), [arXiv:1807.06205 \[astro-ph.CO\]](#).
- [8] T. M. C. Abbott *et al.* (DES), *Mon. Not. Roy. Astron. Soc.* **480**, 3879 (2018), [arXiv:1711.00403 \[astro-ph.CO\]](#).
- [9] A. G. Riess, S. Casertano, W. Yuan, L. M. Macri, and D. Scolnic, *Astrophys. J.* **876**, 85 (2019), [arXiv:1903.07603 \[astro-ph.CO\]](#).
- [10] K. C. Wong *et al.*, (2019), [arXiv:1907.04869 \[astro-ph.CO\]](#).
- [11] W. L. Freedman *et al.*, (2019), [10.3847/1538-4357/ab2f73](#), [arXiv:1907.05922 \[astro-ph.CO\]](#).
- [12] W. Yuan, A. G. Riess, L. M. Macri, S. Casertano, and D. Scolnic, *Astrophys. J.* **886**, 61 (2019), [arXiv:1908.00993 \[astro-ph.GA\]](#).
- [13] C. D. Huang, A. G. Riess, W. Yuan, L. M. Macri, N. L. Zakamska, S. Casertano, P. A. Whitelock, S. L. Hoffmann, A. V. Filippenko, and D. Scolnic, (2019), [arXiv:1908.10883 \[astro-ph.CO\]](#).
- [14] P. A. R. Ade *et al.* (Planck), *Astron. Astrophys.* **571**, A20 (2014), [arXiv:1303.5080 \[astro-ph.CO\]](#).
- [15] H. Bhringer, G. Chon, and C. A. Collins, *Astron. Astrophys.* **570**, A31 (2014), [arXiv:1403.2927 \[astro-ph.CO\]](#).

- [16] N. MacCrann, J. Zuntz, S. Bridle, B. Jain, and M. R. Becker, *Mon. Not. Roy. Astron. Soc.* **451**, 2877 (2015), [arXiv:1408.4742 \[astro-ph.CO\]](#).
- [17] P. A. R. Ade *et al.* (Planck), *Astron. Astrophys.* **594**, A24 (2016), [arXiv:1502.01597 \[astro-ph.CO\]](#).
- [18] S. Joudaki *et al.*, *Mon. Not. Roy. Astron. Soc.* **465**, 2033 (2017), [arXiv:1601.05786 \[astro-ph.CO\]](#).
- [19] H. Hildebrandt *et al.*, *Mon. Not. Roy. Astron. Soc.* **465**, 1454 (2017), [arXiv:1606.05338 \[astro-ph.CO\]](#).
- [20] H. Bhringer, G. Chon, J. Retzlaff, J. Trmper, K. Meisenheimer, and N. Schartel, *Astron. J.* **153**, 220 (2017), [arXiv:1704.06489 \[astro-ph.CO\]](#).
- [21] M. A. Troxel *et al.* (DES), *Phys. Rev.* **D98**, 043528 (2018), [arXiv:1708.01538 \[astro-ph.CO\]](#).
- [22] M. A. Troxel *et al.* (DES), *Mon. Not. Roy. Astron. Soc.* **479**, 4998 (2018), [arXiv:1804.10663 \[astro-ph.CO\]](#).
- [23] N. Aghanim *et al.* (Planck), (2018), [arXiv:1807.06209 \[astro-ph.CO\]](#).
- [24] F. Bianchini *et al.* (SPT), (2019), [arXiv:1910.07157 \[astro-ph.CO\]](#).
- [25] N. Schneberg, J. Lesgourgues, and D. C. Hooper, *JCAP* **1910**, 029 (2019), [arXiv:1907.11594 \[astro-ph.CO\]](#).
- [26] S. Dodelson and L. M. Widrow, *Phys. Rev. Lett.* **72**, 17 (1994), [arXiv:hep-ph/9303287 \[hep-ph\]](#).
- [27] X.-D. Shi and G. M. Fuller, *Phys. Rev. Lett.* **82**, 2832 (1999), [arXiv:astro-ph/9810076 \[astro-ph\]](#).
- [28] Y. Ema and K. Nakayama, *Phys. Lett.* **B776**, 174 (2018), [arXiv:1710.02461 \[hep-ph\]](#).
- [29] R. T. Co, L. J. Hall, and K. Harigaya, *Phys. Rev. Lett.* **120**, 211602 (2018), [arXiv:1711.10486 \[hep-ph\]](#).
- [30] K. Harigaya and J. M. Leedom, (2019), [arXiv:1910.04163 \[hep-ph\]](#).
- [31] B. S. Acharya, K. Bobkov, and P. Kumar, *JHEP* **11**, 105 (2010), [arXiv:1004.5138 \[hep-th\]](#).
- [32] M. Cicoli, J. P. Conlon, and F. Quevedo, *Phys. Rev.* **D87**, 043520 (2013), [arXiv:1208.3562 \[hep-ph\]](#).
- [33] J. P. Conlon and M. C. D. Marsh, *JHEP* **10**, 214 (2013), [arXiv:1304.1804 \[hep-ph\]](#).
- [34] T. Higaki, K. Nakayama, and F. Takahashi, *JHEP* **07**, 005 (2013), [arXiv:1304.7987 \[hep-ph\]](#).
- [35] D. J. E. Marsh, *Phys. Rept.* **643**, 1 (2016), [arXiv:1510.07633 \[astro-ph.CO\]](#).

- [36] T. Moroi, H. Murayama, and M. Yamaguchi, *Phys. Lett.* **B303**, 289 (1993).
- [37] V. S. Rychkov and A. Strumia, *Phys. Rev.* **D75**, 075011 (2007), arXiv:hep-ph/0701104 [hep-ph].
- [38] J. L. Feng, A. Rajaraman, and F. Takayama, *Phys. Rev. Lett.* **91**, 011302 (2003), arXiv:hep-ph/0302215 [hep-ph].
- [39] J. L. Feng, A. Rajaraman, and F. Takayama, *Phys. Rev.* **D68**, 063504 (2003), arXiv:hep-ph/0306024 [hep-ph].
- [40] J. L. Feng, S.-f. Su, and F. Takayama, *Phys. Rev.* **D70**, 063514 (2004), arXiv:hep-ph/0404198 [hep-ph].
- [41] J. L. Feng, S. Su, and F. Takayama, *Phys. Rev.* **D70**, 075019 (2004), arXiv:hep-ph/0404231 [hep-ph].
- [42] J. L. Feng, B. T. Smith, and F. Takayama, *Phys. Rev. Lett.* **100**, 021302 (2008), arXiv:0709.0297 [hep-ph].
- [43] J. L. Feng, Z. Surujon, and H.-B. Yu, *Phys. Rev.* **D86**, 035003 (2012), arXiv:1205.6480 [hep-ph].
- [44] A. Strumia, *JHEP* **06**, 036 (2010), arXiv:1003.5847 [hep-ph].
- [45] K. Rajagopal, M. S. Turner, and F. Wilczek, *Nucl. Phys.* **B358**, 447 (1991).
- [46] L. Covi, J. E. Kim, and L. Roszkowski, *Phys. Rev. Lett.* **82**, 4180 (1999), arXiv:hep-ph/9905212 [hep-ph].
- [47] L. Covi, H.-B. Kim, J. E. Kim, and L. Roszkowski, *JHEP* **05**, 033 (2001), arXiv:hep-ph/0101009 [hep-ph].
- [48] A. Brandenburg, L. Covi, K. Hamaguchi, L. Roszkowski, and F. D. Steffen, *Phys. Lett.* **B617**, 99 (2005), arXiv:hep-ph/0501287 [hep-ph].
- [49] Z. Chacko, H.-S. Goh, and R. Harnik, *Phys. Rev. Lett.* **96**, 231802 (2006), arXiv:hep-ph/0506256 [hep-ph].
- [50] R. Barbieri, T. Gregoire, and L. J. Hall, (2005), arXiv:hep-ph/0509242 [hep-ph].
- [51] R. Barbieri, L. J. Hall, and K. Harigaya, *JHEP* **11**, 172 (2016), arXiv:1609.05589 [hep-ph].
- [52] Z. Chacko, N. Craig, P. J. Fox, and R. Harnik, *JHEP* **07**, 023 (2017), arXiv:1611.07975 [hep-ph].
- [53] N. Craig, S. Koren, and T. Trott, *JHEP* **05**, 038 (2017), arXiv:1611.07977 [hep-ph].

- [54] C. Csaki, E. Kufflik, and S. Lombardo, *Phys. Rev.* **D96**, 055013 (2017), [arXiv:1703.06884 \[hep-ph\]](#).
- [55] R. Barbieri, L. J. Hall, and K. Harigaya, *JHEP* **10**, 015 (2017), [arXiv:1706.05548 \[hep-ph\]](#).
- [56] K. Harigaya, R. McGehee, H. Murayama, and K. Schutz, (2019), [arXiv:1905.08798 \[hep-ph\]](#).
- [57] J. Hasenkamp, *Phys. Lett.* **B707**, 121 (2012), [arXiv:1107.4319 \[hep-ph\]](#).
- [58] E. J. Chun, H. B. Kim, and J. E. Kim, *Phys. Rev. Lett.* **72**, 1956 (1994), [arXiv:hep-ph/9305208 \[hep-ph\]](#).
- [59] K. Ichikawa, M. Kawasaki, K. Nakayama, M. Senami, and F. Takahashi, *JCAP* **0705**, 008 (2007), [arXiv:hep-ph/0703034 \[HEP-PH\]](#).
- [60] K. Hamaguchi, K. Nakayama, and Y. Tang, *Phys. Lett.* **B772**, 415 (2017), [arXiv:1705.04521 \[hep-ph\]](#).
- [61] D. Blas, J. Lesgourgues, and T. Tram, *JCAP* **1107**, 034 (2011), [arXiv:1104.2933 \[astro-ph.CO\]](#).
- [62] B. Audren, J. Lesgourgues, K. Benabed, and S. Prunet, *JCAP* **1302**, 001 (2013), [arXiv:1210.7183 \[astro-ph.CO\]](#).
- [63] T. Brinckmann and J. Lesgourgues, (2018), [arXiv:1804.07261 \[astro-ph.CO\]](#).
- [64] J. Lesgourgues, G. Mangano, G. Miele, and S. Pastor, *Neutrino Cosmology* (Cambridge University Press, 2013).
- [65] G. Mangano, G. Miele, S. Pastor, and M. Peloso, *Phys. Lett.* **B534**, 8 (2002), [arXiv:astro-ph/0111408 \[astro-ph\]](#).
- [66] P. F. de Salas and S. Pastor, *JCAP* **1607**, 051 (2016), [arXiv:1606.06986 \[hep-ph\]](#).
- [67] Z. Hou, R. Keisler, L. Knox, M. Millea, and C. Reichardt, *Phys. Rev.* **D87**, 083008 (2013), [arXiv:1104.2333 \[astro-ph.CO\]](#).
- [68] Z. Chacko, Y. Cui, S. Hong, and T. Okui, *Phys. Rev.* **D92**, 055033 (2015), [arXiv:1505.04192 \[hep-ph\]](#).
- [69] B. Follin, L. Knox, M. Millea, and Z. Pan, *Phys. Rev. Lett.* **115**, 091301 (2015), [arXiv:1503.07863 \[astro-ph.CO\]](#).
- [70] D. Baumann, D. Green, J. Meyers, and B. Wallisch, *JCAP* **1601**, 007 (2016), [arXiv:1508.06342 \[astro-ph.CO\]](#).
- [71] J. Silk, *Astrophys. J.* **151**, 459 (1968).
- [72] W. Hu and N. Sugiyama, *Phys. Rev.* **D51**, 2599 (1995), [arXiv:astro-ph/9411008 \[astro-ph\]](#).

- [73] W. Hu and M. J. White, *Astrophys. J.* **471**, 30 (1996), arXiv:astro-ph/9602019 [astro-ph].
- [74] S. Weinberg, *Cosmology* (2008).
- [75] J. Lesgourgues, in *Proceedings, Theoretical Advanced Study Institute in Elementary Particle Physics: Searching for New Physics at Small and Large Scales (TASI 2012): Boulder, Colorado, June 4-29, 2012* (2013) pp. 29–97, arXiv:1302.4640 [astro-ph.CO].
- [76] K. N. Abazajian *et al.* (CMB-S4), (2016), arXiv:1610.02743 [astro-ph.CO].
- [77] J. L. Bernal, L. Verde, and A. G. Riess, *JCAP* **1610**, 019 (2016), arXiv:1607.05617 [astro-ph.CO].
- [78] K. Aylor, M. Joy, L. Knox, M. Millea, S. Raghunathan, and W. L. K. Wu, *Astrophys. J.* **874**, 4 (2019), arXiv:1811.00537 [astro-ph.CO].
- [79] L. Knox and M. Millea, (2019), arXiv:1908.03663 [astro-ph.CO].
- [80] L. Verde, T. Treu, and A. G. Riess, in *Nature Astronomy 2019* (2019) arXiv:1907.10625 [astro-ph.CO].
- [81] A. Hojjati, E. V. Linder, and J. Samsing, *Phys. Rev. Lett.* **111**, 041301 (2013), arXiv:1304.3724 [astro-ph.CO].
- [82] V. Poulin, T. L. Smith, D. Grin, T. Karwal, and M. Kamionkowski, *Phys. Rev.* **D98**, 083525 (2018), arXiv:1806.10608 [astro-ph.CO].
- [83] V. Poulin, T. L. Smith, T. Karwal, and M. Kamionkowski, *Phys. Rev. Lett.* **122**, 221301 (2019), arXiv:1811.04083 [astro-ph.CO].
- [84] P. Agrawal, F.-Y. Cyr-Racine, D. Pinner, and L. Randall, (2019), arXiv:1904.01016 [astro-ph.CO].
- [85] M. Park, C. D. Kreisch, J. Dunkley, B. Hadzhiyska, and F.-Y. Cyr-Racine, *Phys. Rev.* **D100**, 063524 (2019), arXiv:1904.02625 [astro-ph.CO].
- [86] C. D. Kreisch, F.-Y. Cyr-Racine, and O. Dor, (2019), arXiv:1902.00534 [astro-ph.CO].
- [87] T. L. Smith, V. Poulin, and M. A. Amin, (2019), arXiv:1908.06995 [astro-ph.CO].
- [88] T. Bringmann, F. Kahlhoefer, K. Schmidt-Hoberg, and P. Walia, *Phys. Rev.* **D98**, 023543 (2018), arXiv:1803.03644 [astro-ph.CO].
- [89] K. Vattis, S. M. Koushiappas, and A. Loeb, *Phys. Rev.* **D99**, 121302 (2019), arXiv:1903.06220 [astro-ph.CO].
- [90] D. J. Eisenstein and M. J. White, *Phys. Rev.* **D70**, 103523 (2004), arXiv:astro-ph/0407539 [astro-ph].

- [91] M. A. Buen-Abad, G. Marques-Tavares, and M. Schmaltz, *Phys. Rev.* **D92**, 023531 (2015), [arXiv:1505.03542 \[hep-ph\]](#).
- [92] J. Lesgourgues, G. Marques-Tavares, and M. Schmaltz, *JCAP* **1602**, 037 (2016), [arXiv:1507.04351 \[astro-ph.CO\]](#).
- [93] Z. Chacko, Y. Cui, S. Hong, T. Okui, and Y. Tsai, *JHEP* **12**, 108 (2016), [arXiv:1609.03569 \[astro-ph.CO\]](#).
- [94] M. A. Buen-Abad, M. Schmaltz, J. Lesgourgues, and T. Brinckmann, *JCAP* **1801**, 008 (2018), [arXiv:1708.09406 \[astro-ph.CO\]](#).
- [95] N. Canac, G. Aslanyan, K. N. Abazajian, R. Easther, and L. C. Price, *JCAP* **1609**, 022 (2016), [arXiv:1606.03057 \[astro-ph.CO\]](#).
- [96] S. Joudaki *et al.*, *Mon. Not. Roy. Astron. Soc.* **471**, 1259 (2017), [arXiv:1610.04606 \[astro-ph.CO\]](#).
- [97] P. Ko and Y. Tang, *Phys. Lett.* **B762**, 462 (2016), [arXiv:1608.01083 \[hep-ph\]](#).
- [98] P. Ko and Y. Tang, *Phys. Lett.* **B768**, 12 (2017), [arXiv:1609.02307 \[hep-ph\]](#).
- [99] P. Ko, N. Nagata, and Y. Tang, *Phys. Lett.* **B773**, 513 (2017), [arXiv:1706.05605 \[hep-ph\]](#).
- [100] M. Raveri, W. Hu, T. Hoffman, and L.-T. Wang, *Phys. Rev.* **D96**, 103501 (2017), [arXiv:1709.04877 \[astro-ph.CO\]](#).
- [101] Z. Pan, M. Kaplinghat, and L. Knox, *Phys. Rev.* **D97**, 103531 (2018), [arXiv:1801.07348 \[astro-ph.CO\]](#).
- [102] Z. Chacko, D. Curtin, M. Geller, and Y. Tsai, *JHEP* **09**, 163 (2018), [arXiv:1803.03263 \[hep-ph\]](#).
- [103] M. A. Buen-Abad, R. Emami, and M. Schmaltz, *Phys. Rev.* **D98**, 083517 (2018), [arXiv:1803.08062 \[hep-ph\]](#).
- [104] K. N. Abazajian and A. Kusenko, *Phys. Rev.* **D100**, 103513 (2019), [arXiv:1907.11696 \[hep-ph\]](#).
- [105] L. Maiani, *11th Gif Summer School on Particle Physics: Production and Detection of Heavy Bosons, W⁺-, Z-0 Gif-sur-Yvette, France, September 3-7, 1979*, (1979), [Conf. Proc.C7909031,1(1979)].
- [106] M. J. G. Veltman, *Acta Phys. Polon.* **B12**, 437 (1981).
- [107] E. Witten, *Nucl. Phys.* **B188**, 513 (1981).
- [108] R. K. Kaul, *Phys. Lett.* **109B**, 19 (1982).

- [109] S. Dimopoulos, S. Raby, and F. Wilczek, *Phys. Rev.* **D24**, 1681 (1981).
- [110] S. Dimopoulos and H. Georgi, *Nucl. Phys.* **B193**, 150 (1981).
- [111] N. Sakai, *Z. Phys.* **C11**, 153 (1981).
- [112] L. E. Ibanez and G. G. Ross, *Phys. Lett.* **105B**, 439 (1981).
- [113] M. B. Einhorn and D. R. T. Jones, *Nucl. Phys.* **B196**, 475 (1982).
- [114] W. J. Marciano and G. Senjanovic, *Phys. Rev.* **D25**, 3092 (1982).
- [115] H. Pagels and J. R. Primack, *Phys. Rev. Lett.* **48**, 223 (1982).
- [116] H. Goldberg, *Phys. Rev. Lett.* **50**, 1419 (1983).
- [117] G. 't Hooft, *Phys. Rev. Lett.* **37**, 8 (1976).
- [118] R. D. Peccei and H. R. Quinn, *Phys. Rev. Lett.* **38**, 1440 (1977).
- [119] R. D. Peccei and H. R. Quinn, *Phys. Rev.* **D16**, 1791 (1977).
- [120] S. Weinberg, *Phys. Rev. Lett.* **40**, 223 (1978).
- [121] F. Wilczek, *Phys. Rev. Lett.* **40**, 279 (1978).
- [122] J. Preskill, M. B. Wise, and F. Wilczek, *Phys. Lett.* **120B**, 127 (1983).
- [123] L. F. Abbott and P. Sikivie, *Phys. Lett.* **120B**, 133 (1983).
- [124] M. Dine and W. Fischler, *Phys. Lett.* **120B**, 137 (1983).
- [125] V. A. Kuzmin, M. E. Shaposhnikov, and I. I. Tkachev, *Phys. Rev.* **D45**, 466 (1992).
- [126] G. Servant, *Phys. Rev. Lett.* **113**, 171803 (2014), arXiv:1407.0030 [hep-ph].
- [127] A. Kusenko, K. Schmitz, and T. T. Yanagida, *Phys. Rev. Lett.* **115**, 011302 (2015), arXiv:1412.2043 [hep-ph].
- [128] S. Ipek and T. M. P. Tait, *Phys. Rev. Lett.* **122**, 112001 (2019), arXiv:1811.00559 [hep-ph].
- [129] R. T. Co and K. Harigaya, (2019), arXiv:1910.02080 [hep-ph].
- [130] P. Moxhay and K. Yamamoto, *Phys. Lett.* **151B**, 363 (1985).
- [131] H. Murayama, H. Suzuki, and T. Yanagida, *Phys. Lett.* **B291**, 418 (1992).
- [132] T. Goto and M. Yamaguchi, *Phys. Lett.* **B276**, 103 (1992).
- [133] E. J. Chun, J. E. Kim, and H. P. Nilles, *Phys. Lett.* **B287**, 123 (1992), arXiv:hep-ph/9205229 [hep-ph].
- [134] E. J. Chun and A. Lukas, *Phys. Lett.* **B357**, 43 (1995), arXiv:hep-ph/9503233 [hep-ph].
- [135] J. E. Kim and M.-S. Seo, *Nucl. Phys.* **B864**, 296 (2012), arXiv:1204.5495 [hep-ph].
- [136] M. Kawasaki and K. Nakayama, *Ann. Rev. Nucl. Part. Sci.* **63**, 69 (2013), arXiv:1301.1123 [hep-ph].

- [137] M. Viel, M. G. Haehnelt, and V. Springel, *Mon. Not. Roy. Astron. Soc.* **354**, 684 (2004), [arXiv:astro-ph/0404600](#) [astro-ph].
- [138] P. McDonald *et al.* (SDSS), *Astrophys. J. Suppl.* **163**, 80 (2006), [arXiv:astro-ph/0405013](#) [astro-ph].
- [139] P. McDonald *et al.* (SDSS), *Astrophys. J.* **635**, 761 (2005), [arXiv:astro-ph/0407377](#) [astro-ph].
- [140] A. Boyarsky, J. Lesgourgues, O. Ruchayskiy, and M. Viel, *JCAP* **0905**, 012 (2009), [arXiv:0812.0010](#) [astro-ph].
- [141] D. M. Scolnic *et al.*, *Astrophys. J.* **859**, 101 (2018), [arXiv:1710.00845](#) [astro-ph.CO].
- [142] P. A. Abell *et al.* (LSST Science, LSST Project), (2009), [arXiv:0912.0201](#) [astro-ph.IM].
- [143] R. Laureijs *et al.* (EUCLID), (2011), [arXiv:1110.3193](#) [astro-ph.CO].
- [144] M. P. van Haarlem *et al.*, *Astron. Astrophys.* **556**, A2 (2013), [arXiv:1305.3550](#) [astro-ph.IM].
- [145] L. V. E. Koopmans *et al.*, *Proceedings, Advancing Astrophysics with the Square Kilometre Array (AASKA14): Giardini Naxos, Italy, June 9-13, 2014*, *PoS AASKA14*, 001 (2015), [arXiv:1505.07568](#) [astro-ph.CO].
- [146] D. R. DeBoer *et al.*, *Publ. Astron. Soc. Pac.* **129**, 045001 (2017), [arXiv:1606.07473](#) [astro-ph.IM].
- [147] M. W. Eastwood *et al.*, *Astron. J.* **158**, 84 (2019), [arXiv:1906.08943](#) [astro-ph.CO].
- [148] J. B. Muoz, C. Dvorkin, and F.-Y. Cyr-Racine, (2019), [arXiv:1911.11144](#) [astro-ph.CO].
- [149] T. Banks, M. Dine, and M. Graesser, *Phys. Rev.* **D68**, 075011 (2003), [arXiv:hep-ph/0210256](#) [hep-ph].
- [150] M. Kawasaki and K. Nakayama, *Phys. Rev.* **D77**, 123524 (2008), [arXiv:0802.2487](#) [hep-ph].
- [151] J. Hasenkamp and J. Kersten, *Phys. Rev.* **D82**, 115029 (2010), [arXiv:1008.1740](#) [hep-ph].
- [152] H. Baer and A. Lessa, *JHEP* **06**, 027 (2011), [arXiv:1104.4807](#) [hep-ph].
- [153] K. J. Bae, H. Baer, A. Lessa, and H. Serce, *JCAP* **1410**, 082 (2014), [arXiv:1406.4138](#) [hep-ph].
- [154] R. T. Co, F. D’Eramo, and L. J. Hall, *JHEP* **03**, 005 (2017), [arXiv:1611.05028](#) [hep-ph].
- [155] R. T. Co, F. D’Eramo, L. J. Hall, and K. Harigaya, *JHEP* **07**, 125 (2017), [arXiv:1703.09796](#) [hep-ph].
- [156] N. Arkani-Hamed, A. Delgado, and G. F. Giudice, *Nucl. Phys.* **B741**, 108 (2006), [arXiv:hep-ph/0601041](#) [hep-ph].